CrossMark

Paramagnetic Properties of Fullerene-Derived Nanomaterials and Their Polymer Composites: Drastic Pumping Out Effect

Andriy A. Konchits[1], Bela D. Shanina[1], Serhii V. Krasnovyd[1*], Alexander I. Burya[2] and Olga Yu Kuznetsova[3]

Abstract

The evolution of paramagnetic properties of the fullerene soot (FS), fullerene black (FB), and their polymer composites Phenylon C-2/FS, FB has been studied using the electron paramagnetic resonance (EPR) method. For the first time, a drastic growth of the EPR signals in the FB, FS, and composite samples was observed under pumping out at temperatures $T = 20 \div 300$ °C, which is attributed to the interaction between carbon defects and adsorbed gas molecules, mainly oxygen.

It is shown that the ensemble of paramagnetic centers in the FB, FS, and the composite is heterogeneous. This ensemble consists of three spin subsystems 1, 2, and 3 related with different structural elements. The subsystems give three corresponding contributions, L_1, L_2 and L_3, into the overall contour of the EPR signal. The most intensive and broad signal L_3 is caused by 2D electrons from the surface of carbon flakes. Theoretical calculations of the L_3 signal line shape were carried out, and the decay rate of the integral intensity has been obtained for each component L_1, L_2, and L_3 after the contact of the sample with the ambient air. The signal decay process in the bulk composite samples is much slower due to their low gas permeability at room temperature (RT).

Keywords: Nanomaterials, Fullerene, Electron properties, Paramagnetic oxygen, Carbon defects, Carbon flakes

Background

Carbon-based nanomaterials, such as graphene, nano-tubes, fullerene, onion-like carbon (OLC), nano-diamond (ND), and carbon dots, attract a significant interest of the researchers over the past decade. These materials demonstrate a great variety of their sizes and structures, from small molecules to long chains, as well as variations of the sp^1, sp^2, and sp^3 bond ratio [1]. The unique properties of carbon-based nanomaterials are widely used in many fields, including fundamental material science [1–3], energy [4, 5], biology and medicine [6–9], and environment [10]. Fullerenes and their derivatives occupy the important place among the nanocarbon materials, as well as nano-diamonds and carbon nano-onions (multishell fullerene-type nanostructures). A common property of the nanomaterial group is their ability of mutual transformations, for example, soot or fullerene black to OLC [11, 12], ND in OLC [13], and graphene to fullerene [14].

At present time, the practical application of fullerene materials continues to grow due to new applications in biology [6, 7], medicine [9], synthesis of nanocomposites with unique properties [15, 16], materials for electromagnetic shielding [17–20], and others. The physical-chemical properties of the fullerene-type nanomaterials depend on their electronic properties, the structural imperfection, surface area, and others. For example, the composites of onion-like carbon nanoparticles (their synthesis includes the presence of oxygen) reveal the enhanced microwave-absorption properties [18]. The existence of a huge amount of defects in the fullerene-like materials and deviation of their structure from planarity ("pyramidalization") essentially affect their reactivity [21–24]. The EPR spectroscopy is generally used to get detailed information about the electron properties of fullerene-like materials. The structure and paramagnetic

* Correspondence: krasnovid@inbox.ru
[1]V.E. Lashkaryov Institute for Semiconductor Physics NAS of Ukraine, Kyiv 03028, Ukraine
Full list of author information is available at the end of the article

Konchits *et al. Nanoscale Research Letters* (2017) 12:475

Page 2 of 9

properties of the fullerene soot (FS) and fullerene black (FB) were studied in [25–28]. The EPR signal of these materials is shown to be characterized by the following parameters: $g = 2.0022 \div 2.0023$, $\Delta H_{pp} \cong 2$ G. The concentration of paramagnetic radicals $N_s \sim 10^{21}$ g^{-1} and $N_s \sim 3 \times 10^{18}$ g^{-1} in the initial samples FS [25] and FB [27], has been found, respectively. These parameters are changed insignificantly at the presence of molecular oxygen, except for FB samples, of which the N_s value increases by the order of magnitude after evacuation at $T = 150$ °C [27]. The results obtained for the soot were explained using a model where the fullerene soot particles are assumed to be encapsulated in the highly defective onion-like carbon (OLC) [25].

At the same time, the effect of oxygen on the EPR intensity of radicals is very strong for FB (fullerene-free FS) [27]. The knowledge of the nature and mechanisms for the interaction of the fullerene-like materials with the molecular oxygen remains important, particularly taking into account the results obtained within the recent years [29, 30], where remarkable EPR properties of similar nanocarbon structures were shown to be related with the interaction between paramagnetic centers and gas molecules.

The main aim of our study is to clarify the nature of paramagnetic defects in the fullerene soot and fullerene black, as well as mechanisms of their interaction with molecular oxygen. Furthermore, features of these interactions and the role of polymer matrix will be studied in the composites, based on the aromatic polyamides Phenylon C-2 (PhC-2) which are characterized by strong intermolecular interactions due to hydrogen bonds. Materials like "superplastic" are promising for increase of the heat-resistance and strength in the space technologies. We have previously demonstrated that the presence of fullerene FB and FS fillers, significantly improves mechanical properties of such composites [31]. The different type of fillers is improving electronic properties of the polymer nanocomposites [32].

Methods

Samples C60, fullerene soot, and fullerene black were obtained from NeoTechProduct (Russia, St. Petersburg) and were used as is. According to specification (http://www.neotechproduct.ru/main_page), FS was obtained by means of evaporation of graphite using the arc method. The FS samples are black powder, insoluble with the bulk density of about 0.25 g/cm^3 and the fullerene content of about 10%. FB samples are a powder product after extraction of fullerenes from FS. Extraction is carried out with the help of nonpolar organic solvent (o-xylol) and post-treatment with steam to remove organic solvent. The fullerene C60 content in the FB samples is ≤0.3%.

The original polymer matrix PhC-2 is the linear heterocyclic copolymer containing in its macromolecule's main chain the –HNCO– amide group linked at both sides by phenile fragments. It has been obtained by means of emulsion polycondensation of metaphenilenediamine supplemented by the mixture of dichloranhydrides of isophtale and terephtale acids which were taken in the molar ratio of 3 to 2.

The composites PhC-2/FS and FB were obtained by means of mixing the components in the rotating electromagnetic field with further treatment of the compositions by the compression molding method ($T = 598$ K, $P = 40$ MPa). The filler amount in compositions was 1.5 and 3 wt.%.

Magnetic resonance measurements were carried out at room temperature mainly using the X-band (microwave frequency $\nu \sim 9.4$ GHz) EPR spectrometer Radiopan X-2244 with 100 kHz modulation of magnetic field. The estimated accuracy in the determination of the g-factor was $\pm 2 \times 10^{-4}$ for the observed EPR lines with linewidth $\Delta H_{pp} \leq 10$ G. The absolute accuracy of the spin density (N_s) was ±50%, whereas the relative accuracy of N_s was ±20%. The paramagnetic properties of the samples were studied in the ambient air, as well as under conditions of the controlled oxygen concentration using the pumping out at $T = 20 \div 170$ °C. The samples were placed into a quartz tube which was evacuated at the definite temperature. Then, the samples have been put into the cavity of the spectrometer, and EPR spectrum was recorded without change of the pumping out conditions.

Results and Discussion

Figure 1a demonstrates the EPR spectra of fullerene C60, fullerene soot, and fullerene black at room temperature. Within the experimental error, all the spectra are characterized by g-factor $g = 2.0024 \pm 2 \times 10^{-4}$. The line shape is the Lorentzian only for the sample C60, whereas it is described by the sum of two Lorentz lines for the FS and FB samples. The spin concentration and the contribution of individual components to the total intensity of the spectrum are shown in Table 1 for these and other samples studied. The insert in Fig. 1a shows the EPR spectrum FB sample at $T = 30$ K. Parameters of this spectrum are given also in Table 1.

Figure 1b presents the ESR spectra of composites Phenylon C-2 with 3% of C60 (1), FS (2), and FB (3) as the fillers. The insert in Fig. 1b shows the spectrum of the composite PhC-2/FB at $T = 30$ K. Parameters obtained as a result of fitting the calculated signals to the experimental one are given in Table 1. Properties of composite samples and their fillers were also studied under evacuation at different temperatures within the range of $T = 20 \div 300$ °C.

Konchits *et al. Nanoscale Research Letters* (2017) 12:475

Page 3 of 9
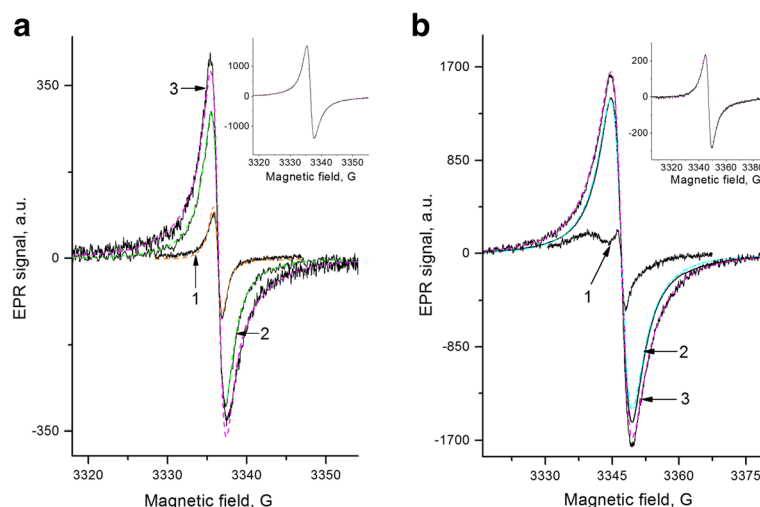
Fig. 1 EPR spectra of fullerene, FS, FB, and composites Phenylon C-2/FS, FB. **a.** *1*—initial samples of the fullerene C60, *2*—fullerene soot (FS), *3*—fullerene black (FB) at room temperature. *Dashed lines* are the calculated signals (Table 1). v = 9350 MHz. The insert: EPR spectrum of the fullerene black at T = 30 K. **b.** Composites Phenylon C-2 + 3% fillers, notably: *1*—fullerene C60, *2*—fullerene soot (FS), *3*—fullerene black (FB). The supplementary broad line on the spectrum (1) belongs to Phenylon C-2. v = 9375 MHz, gain = ×5. The insert: The EPR spectrum of the composite PhC-2 + 3% FS at T = 30 K. *Dashed lines*—fitting (Table 1)

Table 1 EPR characteristics of studied samples

Sample	N_s, cm^{-3a}	The contribution of the components in the total spectra intensity
Fullerene C60		
C60	~5 × 10^{15}	Pure Lorentzian, ΔH = 0.9 G
Pump. at RT	−−//−−	No pumping out effect
Fullerene soot		
On air	~1.8 × 10^{17}	0.49 [ΔH_1 = 1.5 G] + 0.51 [ΔH_2 = 4.2 G]
In pure O_2	~1.5 × 10^{17}	0.26 [ΔH_1 = 1.3 G] + 0.74 [ΔH_2 = 3 G]
RT pump.	1.7 × 10^{18}	0.11 [ΔH_1 = 1.2 G] + 0.89 [ΔH_2 = 5.8 G]
Pump. at 150 ℃	6.4 × 10^{18}	0.03 [ΔH_1 = 0.9 G] + 0.13 [ΔH_2 = 2.4 G] + 0.84 [ΔH_3 = 10 G]
Pump. at 550 ℃	1.6 × 10^{19}	0.59 [ΔH_1 = 8.2 G] + 0.41 [ΔH_2 = 22 G]
After 24 h on air	1.9 × 10^{19}	0.65 [ΔH_1 = 6.9 G] + 0.35 [ΔH_2 = 22 G]
Fullerene black		
On air	2.4 × 10^{17}	0.3 [ΔH_1 = 1.6 G] + 0.7 [ΔH_2 = 5.5 G]
In He gas, T = 30 K	~9 × 10^{17}	0.32 [ΔH_1 = 2.0 G] + 0.68 [ΔH_2 = 6.5 G]
RT pumping	1.9 × 10^{18}	0.35 [ΔH_1 = 2.55 G] + 0.65 [ΔH_2 = 6.0 G]
Pump. at 150 ℃	8.0 × 10^{18}	0.25 [ΔH_1 = 2.0 G] + 0.75 [ΔH_2 = 6.5 G]
Pump. at 300 ℃	1.2 × 10^{19}	0.006 [ΔH_1 = 0.9 G] + 0.06 [ΔH_2 = 3.0 G] + 0.93 [ΔH_3 = 24 G]
Composite Phenylon C-2 + 3% fullerene soot		
On air	8 × 10^{15}	0.39 [ΔH_1 = 2.2 G] + 0.61 [ΔH_2 = 6 G]
Pump. at 160 ℃	3.5 × 10^{16}	0.3 [ΔH_1 = 2.3 G] + 0.7 [ΔH_2 = 7 G]
Composite Phenylon C-2 + 3% fullerene black		
On air	1.2 × 10^{16}	0.39 [ΔH_1 = 3.8 G] + 0.61 [ΔH_2 = 9 G]

^{a}The apparent density is used for filler

Figure 2a shows the EPR spectra of FS in the pumping out conditions. It is seen that the intensity of the spectrum significantly increases with increasing of vacuum due to the pumping out at RT. It is obtained that the pumping out of the FS samples at higher temperatures causes a drastic increase in signal intensity by more than 30 times in comparison with the signal in the initial samples, mainly due to formation of the broad wings of the EPR spectrum (Fig. 2a, see data of fitting in Table 1). A similar effect, though not so strong, is observed in the composites after pumping out of samples at the elevated temperatures (Fig. 2b, see data of fitting in Table 1).

The rate of the signal recession (restoration of equilibrium) has been studied for FB sample after cessation of pumping at T = 300 ℃ and bringing the sample in contact with ambient air. This process was studied in detail for each of the three spectral components L_1, L_2, and L_3, as shown in Fig. 3. It should be noted that the contribution of the components L_3 was determined taking into account the properties of 2D electron spin subsystem (see the "Discussion" below).

The decay of these signal intensities with holding time of contacting the sample with the ambient atmosphere is shown in Fig. 4. At first, the main part of the signal decay for each component occurs for a short time (from few seconds to 1 min). Thereafter, a much slower decline (for a few hours) takes place until the recovery to the original equilibrium state of the sample.

A similar behavior for powder composite samples ($d \sim 150$ μ) is observed. However, it is different for the bulk samples. Figure 5 shows the time dependence of decline for the full signal intensity of the composite sample PhC-2 +

3% FS ($\sim 1.5 \times 3 \times 3$ mm^3) after pumping out at T = 160 ℃ and following contact with air. One can see from the comparison of Figs. 4 and 5 that the characteristic decay time of the signal intensity for the bulk composite sample is by more than one order of magnitude as large as it is the case for the powder composite and filler samples.

For a more detailed characterization of thermal behavior of materials under study, the annealing (in a weak vacuum) of sample FS was carried out at T = 550 ℃. The recorded spectra are shown in Fig. 6. It is seen that paramagnetic properties of the annealed at T = 550 ℃ samples differ greatly from the properties of the unannealed samples, namely, the subsequent pumping out of the annealed sample does not lead to any drastic changes in the ESR spectrum neither in the line shape nor in the total signal intensity. Figure 6 and Table 1 show that the line shape of the spectrum is determined mainly by the Lorentzian line shape with linewidth ΔH = 7÷8 G in both cases, and intensity of the spectrum is almost independent of pumping. This behavior is very different from that shown in Fig. 4, as well as on the paramagnetic behavior of fullerene black samples annealed at T = 850 ℃ [27]. Such difference is most likely due to the fact that temperatures of 550 ℃ do not refer to the "low-temperature" but to the "mid-temperature" interval of temperature treatments of carbon materials, when their paramagnetic characteristics change significantly [33, 34]. Figure 6 illustrates this fact.

Discussion

Paramagnetic centers in the initial FS and FB samples were observed with their concentration of $2 \cdot 10^{17}$ cm^{-3} and g-value of 2.0024 ± 2 × 10^{-4}, i.e., close to that for
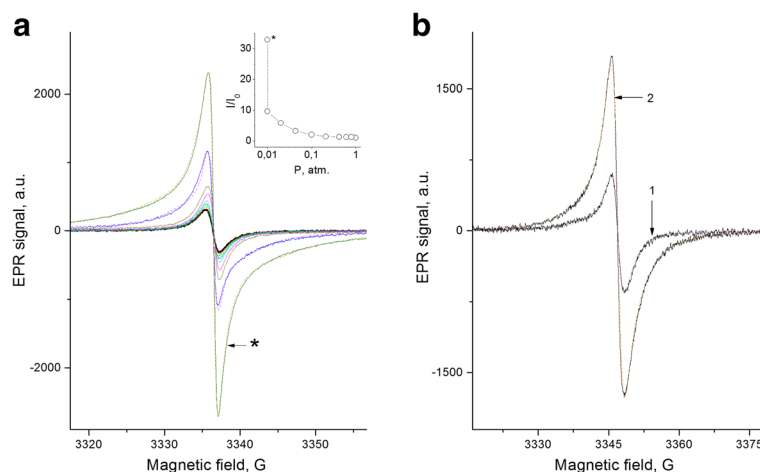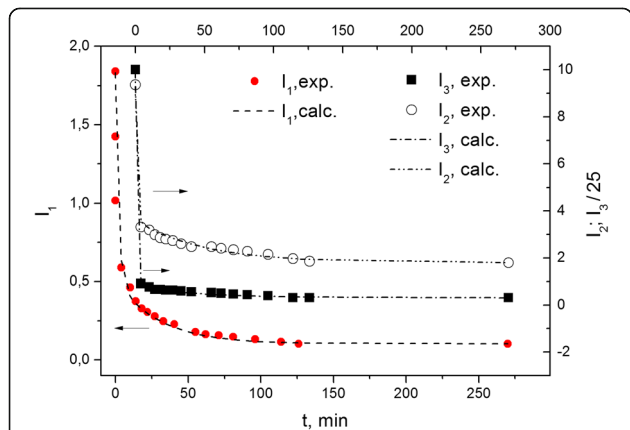

Fig. 2 EPR spectra of fullerene soot at the various oxygen content and composite PhC-2 + 3% fullerene soot. **a.** The magnitude of the pressure of residual atmospheres (from the small to the larger amplitudes of the EPR spectrum) at room temperatures of pumping out: 1; 0.8; 0.61; 0.42; 0.21; 0.1; 0.043; 0.02; 0.001 atm., *—pump. 0.5 h at 160 ℃, *dash line*—fitting by 3 Lorentzian. The insert: the dependence of the total intensity of the EPR spectrum on the oxygen pressure. *—pumping out 0.5 h at T = 160 ℃. **b.** The composite PhC-2 + 3% fullerene soot (FS) before (1) and after (2) pumping out of the samples during 1 h at T = 160 ℃. *Dashed lines*—fitting (Table 1)

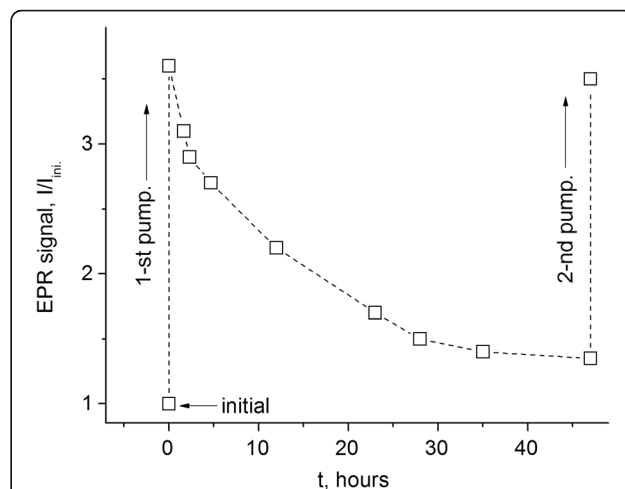Konchits *et al. Nanoscale Research Letters* (2017) 12:475

Page 5 of 9
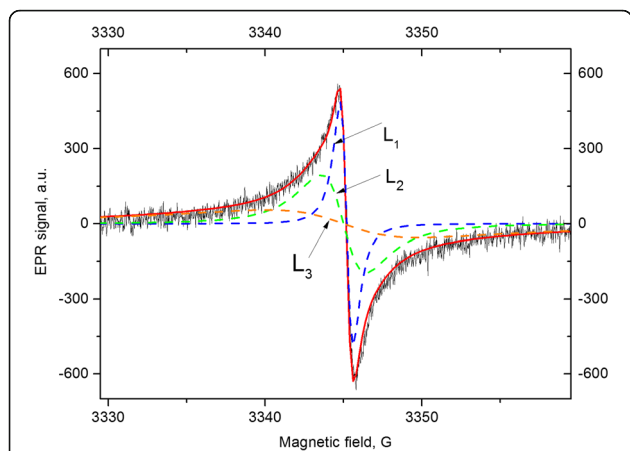
Fig. 3 The separation of the EPR spectrum into components. The sample FB after pumping out during 0.5 h at $T = 300$ ℃. L_1, L_2, and L_3—components of the spectrum with $\Delta H = 0.9$, 3.0, and 24 G respectively. The *solid red line* is the envelope of spectrum. L_3 component was calculated taking into account subsystem of 2D electrons. $v = 9375$ MHz

Fig. 5 The decline of the EPR signal of the bulk composite sample PhC-2 + 3% FS ($d \sim 1.5 \times 3 \times 3$ mm^3) after evacuation during 1 h at $T = 160$ ℃. The contact of the sample was set with the environment after evacuation

paramagnetic defects in many carbonaceous materials, e.g., coal [35] or graphene [36]. In case of the pumping out the FS and FB samples, particularly at the elevated temperatures, the PC concentration increases more than 30 times, up to 1.2×10^{19} cm^{-3}, (see Fig. 2a and Table 1). Before discussing the origin of the PC and the reason for the drastic pumping out effect, let us analyze in detail the evolution of the signals and the line shape of the EPR spectrum under these conditions.

The material under study was a mixture of three-dimensional fullerene-like objects and 2D unclosed carbon flakes of various shapes. Therefore, in our analysis, we should also take into account the presence of spins localized on the open and flat objects belonging to the two-dimensional (2D) electron system.

Contributions of 2D Spin System to the EPR Spectrum

Description of the experimental signals was carried out using the sum of two Lorentzians L_1 and L_2 for three-dimensional paramagnetic systems and the theoretical EPR signal L_3 for the diluted 2D spin system of 2D electrons at the carbon flakes. The latter was found in [37–39] as the Fourier image of free induction decay.

$$L_3(w) = I_0 \cdot \int_{-\infty}^{\infty} \exp\left(-(t/T_2)^{2/3} \exp(i(\omega-\omega_0)t)dt\right)$$

(1a)

Fig. 4 The decline of the intensity of the EPR spectrum components L_1, L_2, and L_3 after the contact of the sample with the air. Start time $t = 0$ corresponds to the condition of the Fig. 3
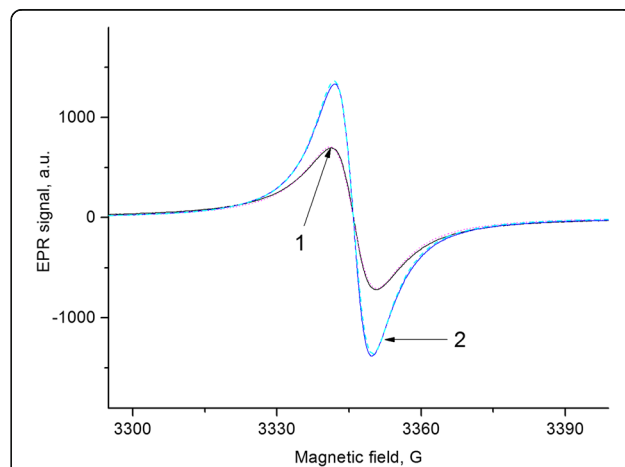

Fig. 6 The EPR spectrum of FS sample. *1*—The sample of FS was annealed 1 h at $T = 550$ ℃ in the low vacuum, *2*—the sample of FS was stored 24 h in the ambient air after annealing

Konchits *et al. Nanoscale Research Letters* (2017) 12:475

Page 6 of 9

$$F(\omega) = L_1(\omega) + L_2(\omega) + L_3(\omega), \tag{1b}$$

The signals in (1b) are written in the order of increasing linewidth. In the experiment, the resonance signals were recorded as a derivative of the absorption signal. Therefore, the derivative of $F(\omega)$ consists of two derivatives of the Lorentz functions, which are well known, whereas the $L'_3(\omega)$ is calculated as a derivative of the absorption signal (1a). The derivatives can be written as follows:

$$L'_1(\omega) + L'_2(\omega) = -2^*A_1{}^*z_1/\left(1 + z_1^2\right)^2 - 2^*A_2{}^*z_2/$$

$$\left(1 + z_2^2\right)^2, \text{ where } z_{1,2} = (\omega - \omega_{1,2})/\Delta_{1,2} \tag{2}$$

$$L'_3(\omega) = -A_3{}^*\Delta_{3^{-1}}{}^* \int \exp\left(-x^2\right)^* x^{5*} \sin\left(z_3{}^*x^3\right) dx,$$

$$\text{where } z_3 = (\omega - \omega_3)/\Delta_3, \quad x = t^{1/3} \tag{3}$$

Integration in (3) is done numerically.

Figure 7 illustrates the comparison of the width and line shape for the Lorentzian and calculated signal from Eq. (1a). One can see that the signal for the 2D system is narrower than the Lorentzian absorption signal in the center and wider at its wings. As a result of the computation of (1a), (1b), (2), and (3) with the following fitting to the experimental spectrum, the amplitudes A_i, the resonance fields ω_{0i}, and the width of signals $\Delta_i = 1, 2, 3$ have been found.

Figure 3 represents a good consistency between the experimental spectrum and the calculated spectrum

Fig. 7 Comparison of absorption signals of the Lorentz shape (*dotted line*) with the line shape for the 2D system (*solid line*) with unit amplitudes and widths of signals
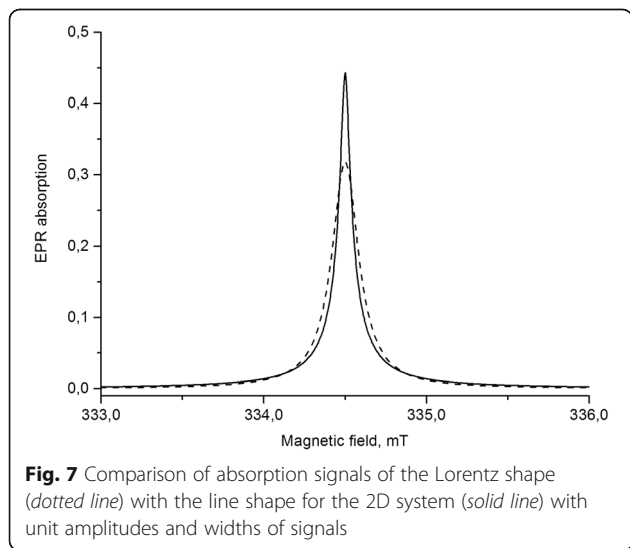
including two Lorentzian derivatives plus the resonance signal of two-dimensional spin system. Therefore, after the sample pumping out, three spin subsystems contribute to the spectrum with the resonance signals L_1, L_2 and L_3, each of which decreases with time after bringing the sample into contact with the environment (Fig. 4). The comparative contributions of three subsystems can be seen in Fig. 3 and are presented in Table 1.

Lorentzian L_1 has the constant g-factor of 2.0024, the smallest linewidth equal to 0.9 G, and the amplitude of the signal which changes by an order of magnitude in dependence of the holding time in the air. The small width of the line L_1 shows its isolation from other spin systems. A similarity of its g-factor and the g-factor of the defects in the fullerene indicates that paramagnetic centers of this subsystem belong to fullerene-like three-dimensional objects. The higher concentration of the centers responsible for the L_1 signal, compared with the pure fullerene C60, should not be surprising. It is known [40] that this signal belongs to $C_{120}O$ defects, whose concentration sharply increases upon annealing the samples at temperatures of ~100 ÷ 200 °C, which is the case in our experiments. Second Lorentz signal L_2 is characterized by three times larger signal width in comparison with the L_1 signal and has a g-factor of 2.0025. The conclusion about the nature of this subsystem will be made after discussing the integral intensities and their decay with holding time in the air, t_{air}. It is worth noting only that all the amplitudes are changed by the order of magnitude in the course of holding in the air. The L_3 signal from the two-dimensional electron spin system has the greatest width and a g-factor of 2.0025. In contrast to other two subsystems, the L_3 signal width changes from 25 to 16.5 G. The large signal width and its decrease with the decrease of spin concentration during holding time t_{air} suggest that the dipole-dipole interaction between the spins determines the linewidth. Its value of 20 G corresponds to the average distance between the spins of about 1 nm. Carbon flakes have a size of about 10 to 100 nm, so that each flake can contain several uncompensated spins.

The integral intensities have been obtained and their dependence versus the holding time t_{air} in air is shown in Fig. 4. A common feature of all the subsystems is a rapid change in the concentration of the spin on the first stage, where $t_{air} \leq 1$ min and a slow concentration decline thereafter. As seen from Fig. 4, the decrease in the integral intensity of L_1 signal is smoother in comparison with that for signals L_2 and L_3. Its main change in the air proceeds in tens of seconds, whereas further change continues for hours. The dependence of the integral intensities of the time t_{air} is described by two exponential functions for all signals:

Konchits *et al. Nanoscale Research Letters* (2017) 12:475

Page 7 of 9

$$I_1(t_{\text{air}}) = 0.152 \cdot \left(1 + 13 \cdot \exp\left(-\frac{t}{2}\right) + 4 \cdot \exp\left(-\frac{t}{30}\right) \right);$$

$$I_2(t_{\text{air}}) = 1.38 \cdot \left(1 + 4 \cdot \exp\left(-\frac{t}{1}\right) + 1 \cdot \exp\left(-\frac{t}{50}\right) \right);$$

$$I_3(t_{\text{air}}) = 0.21 \cdot \left(1 + 30 \cdot \exp\left(-\frac{t}{0.8}\right) + 1.5 \cdot \exp\left(-\frac{t}{50}\right) \right).$$

The decay time is the shortest for the two-dimensional spin system, $\tau_3 = 0.8$ min. From the analysis of the spectra, it was found that the change in the spin concentration of the two-dimensional system, as determined by the integral intensity of the L_3 signal, is accompanied by the variation of signal width, whereas the width of signals L_1 and L_2 remains unchanged when their integral intensity, i.e., spin concentration, varies. This confirms the spin-spin mechanism for the broadening of a two-dimensional signal. The rapid initial decline of the intensities I_3 and I_2 is explained by the easy accessibility of these subsystems for the gas particles, e.g., oxygen, in contrast to twice a slower decline in I_1 for subsystem 1, whose spins are encased in the fullerene-like three-dimensional structures and less available for diffusing particles. Spin concentration of subsystem 1 is small and corresponds to the estimated concentration of fullerene-like particles in the sample. Subsystem 2, which is open for the gas molecules and has a lower concentration compared to the 2D subsystem 3, most likely belongs to the uncompensated spins of carbon bonds of the edge atoms at carbon sheets.

The Nature of the EPR Signals and the Role of Molecular Oxygen
The nature of paramagnetic defects of carbonaceous materials (carbon nano-onion, graphene, fullerenes and fullerene-derived materials, astra lens, and so on) has been widely discussed over the past decade [23–31, 33–36, 41]. Fullerenes can contain defects of molecules C60 [40, 42], FS, and FB—uncompleted sp^2—or sp^3 valences, e.g., the edges of carbon fragments [25–27, 36] or localized spins attributed to sp^3 dangling bonds between neighboring carbon sheets [29]. It is well known, that the molecular oxygen localized near carbon dangle bonds causes a noticeable broadening of the EPR signal. The quantitative dependence of the linewidth on the concentration O_2 molecules was studied in detail in [35, 43]. As seen from Table 1, all fullerene-like materials do not reveal the effect of the air on the linewidth in the EPR spectra. Moreover, the widest component L_3 is narrowing in the course of the long time holding in the air. Therefore, the role of the molecular oxygen in the studied here materials is quite different, if it generally exists.

Let us compare the properties of different fullerene-like samples after the pumping out as given in Table 1. The third column shows the relative contributions of three spin subsystems to the EPR spectra. It calls attention the fact that the narrowest signal L_1 exists in all the samples including the pure fullerene, where L_1 belongs to the only spin subsystem. This spin system is specific for the carbon dangling bonds belonging to fullerene molecule with the structural defects. The L_1 contribution is not higher than 30% for all fullerene-like samples after pumping out. Signals L_2 and L_3 appear just after pumping out. It is worth noting that spin subsystem 2 is observed at any temperature of pumping in contrast to spin subsystem 3. It says about a difference between these systems in the binding energy between the evacuated molecules and the carbon atom. The spin subsystem 2 is characterized by the smallest binding energy, which we attribute to the edge carbon atoms at the carbon flakes. In fact, the smallest binding energy exists between carbon atoms located at the nearest flake-neighbors and it is being broken under pumping out. Spin subsystem 3 is characterized by the largest spin concentration (by $2 \div 3$ order as large as spin concentrations for subsystems 1 and 2), which results in the largest linewidth and the line shape typical for 2D spin subsystems. This suggests that spin subsystem 3 belongs to dangling carbon bonds at the surface of carbon flakes. This subsystem is observed mainly at the pumping temperature $T \geq 100$ °C and its contribution is larger if the pumping temperature increases up to $T = 300$ °C. It means that the binding energy for these carbon atoms with gas molecules is larger than for the edge atoms.

In our experiments, we did not observe either the broadening of L_1, L_2, and L_3 signals caused by oxygen, or a very broad EPR line. However, recently, such EPR line with $\Delta H \geq 200$ G was observed in the oxidized graphene [44]. In [44], the narrow ESR line of carbon defects with $g = 2.002$ was gradually restored in contact with nitrogen gas, which substituted the oxygen, and this process has reached saturation after about 10 min of holding under nitrogen.

We observe also a significant change in the properties of the samples during annealing the fillers at an elevated temperature (Fig. 6 and Table 1), which indicates on the modification of the material structure. This result is consistent with the data [25, 27], where a change was also observed in the structure of the FS [25] and paramagnetic properties of FB [27] in the course of high-temperature annealing.

EPR in the Composite Phenylon C-2/Fullerene Soot
It is seen from Fig. 1a, b, as well as in Table 1, that the width of the lines of individual components in the EPR spectrum of the composite is greater than their value for

Konchits *et al. Nanoscale Research Letters* (2017) 12:475

Page 8 of 9

the filler. Moreover, a broader component of spectrum is dominant (0.61) in the composite, and the width value $\Delta H_2 = 6$ G is close to the value for the pumped out FS sample (Table 1). This seems to be not surprising if to take into account that the conventional cooking process of the composite takes place at $T = 325$ °C and the gas content in the melt is not controlled. The effect of pumping out the composite at $T = 160$ °C (Fig. 2b) is much weaker than it occurs separately for the filler (Fig. 2a), which is clearly associated with a much worse gas permeation in the composite in comparison with that for the filler. For the same reason, the rate of decay of the EPR signal in the composite is significantly reduced after evacuation at $T = 160$ °C, by more than an order of magnitude, if thereafter the sample is brought in contact with the air (compare Figs. 4 and 5). The fast exponent of the signal decay (~1 min) is absent (see Fig. 5), because the process is almost entirely controlled by slow rate of oxygen penetration into the sample.

Conclusions

Fullerene soot and fullerene black actively interact with gas molecules from the environment. This leads to an almost complete (about 95%) suppression of EPR signals from carbon defects, which can be restored after pumping out the samples in the temperature range of 20 to 300 °C. Under these conditions, a complex EPR spectrum consisting of three components, each of which originated from the specific elements of the sample structure, is clearly manifested. The most powerful contribution L_3 comes from the 2D electron spin subsystem at the surface of the carbon flakes. The L_1 and L_2 components belong to defects of fullerene (or fullerene-like) molecules and edge carbon atoms at the carbon flakes. Theoretical calculations of the L_3 signal line shape were carried out and a good agreement with experiment has been obtained. The decay rate of the L_1, L_2, and L_3 components in the total EPR signal (the restoration of equilibrium), after bringing the sample into contact with the ambient air was obtained from the comparison with the experiment.

These phenomena occur also in the bulk of composite samples Phenylon C-2/FS, FB. However, they are observed not so clear, which is possibly due to other prehistory of samples, as well as to the apparent low gas permeability of composites at RT.

It remains questionable whether the carbon dangling bonds are "killed" in contact with the adsorbed gas for the short time ($t_{air} \sim 1$ s) between the end of pumping out and the first EPR registration in the ambient air or their EPR signal becomes greatly broadened and unobservable due to the contact with paramagnetic oxygen. Finally, we believe that the highly absorbent structures, as described above, may find their use in environmental studies, as well as oxygen sensors in biomedicine.

Author details
[1]V.E. Lashkaryov Institute for Semiconductor Physics NAS of Ukraine, Kyiv 03028, Ukraine. [2]Dniprodzerzhynsk State Technical University, Dniprodzerzhinsk 51918, Ukraine. [3]Dnipropetrovsk State Agrarian and Economic University, Dnipropetrovsk 49600, Ukraine.

References
1. Georgakilas V, Perman JA, Tucek J, Zboril R (2015) Broad family of carbon nanoallotropes: classification, chemistry, and applications of fullerenes, carbon dots, nanotubes, graphene, nanodiamonds, and combined superstructures. Chem Rev 115:4744–4822
2. Novoselov KS, Geim AK, Morozov SV, Jiang D, Zhang Y, Dubonos SV, Grigorieva IV, Firsov AA (2004) Electric field effect in atomically thin carbon films. Science 306(5696):666–669

Konchits *et al. Nanoscale Research Letters* (2017) 12:475

Page 9 of 9

3.   Brus DM, Mykhailiv O, Echegoyen L, Plonska-Brzezinska ME (2016) Carbon Nano-Onions. In: Carbon Nanomaterials Sourcebook; Graphene, Fullerenes, Nanotubes, and Nanodiamonds. editor. Sattler KD, CRC Press; 275–302
4.   Rashid bin Mohd Yusoff A. Graphene-based Energy Devices. Wiley: VCH; 2015.
5.   Sun H, You X, Deng J, Chen X, Zhibin Y, Ren J, Peng H (2014) Novel graphene/carbon nanotube composite fibers for efficient wire-shaped miniature energy devices. Adv Mater 18:2868–2873
6.   Bandi R, Gangapuram BR, Dadigala R, Eslavath R, Singh SS, Guttena V. Facile and green synthesis of fluorescent carbon dots from onion waste and their potential applications as sensor and multicolour imaging agents. RSC Adv. 2016; doi:10.1039/C6RA01669C
7.   Ghosh M, Sonkar SK, Saxena M, Sarkar S (2011) Carbon nano-onions for imaging the life cycle of drosophila Melanogaster. Small 22:3170–3177
8.   Wu L, Cai X, Nelson K, Xing W, Xia J, Zhang R, Stacy AJ, Luderer M, Lanza GM, Wang LV, Shen B, Pan D. A green synthesis of carbon nanoparticles from honey and their use in real-time photoacoustic imaging. Nano Res. 2013; doi: 10.1007/s1227401303088.
9.   Zeynalov EB, Allen NS, Salmanova NI (2009) Radical scavenging efficiency of different fullerenes C60–C70 and fullerene soot. Polym Degrad Stab 94: 1183–1189
10. Adeli M, Soleyman R, Beiranvand Z, Madani F. Carbon nanotubes in cancer therapy: a more precise look at the role of carbon nanotube-polymer interactions, Chem Soc Rev. 2013; doi: 10.1039/c3cs35431h.
11. Heer de WA, Ugarte D (1993) Carbon onions produced by heat treatment of carbon soot and their relation to the 217.5 nm interstellar absorption feature. Chem Phys Lett 4:480–486
12. Ugarte D (1994) High-temperature behaviour of "fullerene black". Carbon 7: 1245–1248
13. Kuznetsov VL, Chuvilin AL, Butenko YV, Malkov IY, Titov VM (1994) Onion-like carbon from ultra-disperse diamond. Chem Phys Lett 4:343–348
14. Chuvilin A, Kaiser U, Bichoutskaia E, Besley NA, Khlobystov AN (2010) Direct transformation of graphene to fullerene. Nat Chem 2:450–453
15. Stankovich S, Dikin DA, Dommett GH, Kohlhaas KM, Zimney EJ, Stach EA, Piner RD, Nquyen ST, Ruoff RS (2006) Graphene-based composite materials. Nature 442:282–286
16. Fals AE, Hadjiev VG, Hernandez Robles FC (2012) Multi-functional fullerene soot/alumina composites with improved toughness and electrical conductivity. Mater Sci Eng A 558:13–20
17. Macutkevic J, Kuzhir P, Seliuta D, Valusis G, Banys J, Paddubskaya A, Bychanok D, Slepyan G, Maksimenko S, Kuznetsov V, Moseenkov S, Shenderova O, Mayer A, Lambin P (2010) Dielectric properties of a novel high absorbing onion-like-carbon based polymer composite. Diam Relat Mater 19:91–99
18. Jiang L, Wang Z, Geng D, Yangning L, Yu W, Jing A, Jun H, Da L, Wei L, Zhidong Z (2015) Structure and electromagnetic properties of both regular and defective onion-like carbon nanoparticles. Carbon 95:910–918
19. Chung DDL (2012) Carbon materials for structural self-sensing, electromagnetic shielding and thermal interfacing. Carbon 50:3342–3353
20. Kornienko NE, Naumenko AP (2015) Collective Nature of Chemical Bonds in Fullerenes and Fullerites C60. editor. Thakur VK, Thakur MK, CRC Press; 103–138
21. Sola M, Mestres J, Duran M (1995) Molecular size and pyramidalization: two keys for understanding the reactivity of fullerenes. J Phys Chem 27:10752–10758
22. Werner H, Herein D, Blocker J, Henschke B, Tegtmeyer U, Schedel-Niedring T, Keil M, Bradshaw AM, Schlogl R (1992) Spectroscopic and chemical characterization of "fullerene black". Chem Phys Lett 1:62–66
23. Cataldo F (2002) The impact of a fullerene-like concept in carbon black science. Carbon 40:157–162
24. Hirsch A, Brettreich M (2005) Principles and Perspectives of Fullerene Chemistry. In: Fullerenes: Chemistry and Reactions. editors. Hirsch A, Brettreich M, WILEY; 383–415
25. Dunne LJ, Sarkar AK, Kroto HW, Munn J, Kathirgamanathan P, Heinen U, Fernandez J, Hare J, Reid DG, Clark AP (1996) Electrical, magnetic and structural characterization of fullerene soots. J Phys Condens Matter 8:2127–2141
26. Dunne LJ, Nolan PF, Munn J, Terrones M, Jones T, Kathirgamanathan P, Fernandez J, Hudson AD (1997) Experimental verification of the dominant influence of extended carbon networks on the structural, electrical and magnetic properties of a common soot. J Phys Condens Matter 9:10661–10673
27. Kulikov AV, Kushch SD, Fursikov PV, Bogatyrenko VR (2002) ESR study of fullerene black. Appl Magn Reson 22:539–550
28. Kushch SD, Kuyunko NS (2011) Fullerene black: structure, properties and possible applications. Russ J Gen Chem 2:345–353
29. Shames AI, Osipov VY, AYa V, Kaburagi Y, Hayashi T, Takai K, Enoki T (2013) Spin–spin interactions between π- electronic edge-localized spins and molecular oxygen in defective carbon nano-onions. Carbon 61:173–189
30. Boukhvalov DW, Osipov VY, Shames AI, Takai K, Hayashi T, Enoki T (2016) Charge transfer and weak bonding between molecular oxygen and graphene zigzag edges at low temperatures. Carbon 107:800–810
31. Burya A, Kuznetsova O, Konchits A, Redchuk A (2011) The influence of nanocluster carbon materials on the structure and properties of polyamide nanocomposites. Mater Sci Forum 674:189–193
32. Prateek TVK, Gupta RK (2016) Recent progress on ferroelectric polymer – based nanocomposites for high energy density capacitors: synthesis, dielectric properties, and future aspects. Chem Rev 116:4260–4317
33. Singer LS (1963) A Review of Electron Spin Resonance in Carbonaceous Materials. Proceedings of the Fifth Conference on Carbon 2:37–64 Pergamon Press, N-Y
34. Mrozowski S (1988) ESR studies of carbonization and coalification processes Part I: carbonaceous compounds. Carbon 26(4):521–529
35. Konchits AA, Shanina BD, Valakh MYA, Yanchuk IB, Yukhymchuk VO, Alexeev AD, Vasilenko TA, Molchanov AN, Kirillov AK. Local structure, paramagnetic properties, and porosity of natural coals: spectroscopic studies. J Appl Phys. 2012; doi: 10.1063/1.4745015.
36. Augustyniak-Jabłokow MA, Tadyszak K, Mackowiak M, Lijewski S (2013) ESR study of spin relaxation in graphene. Chem Phys Lett 557:118–122
37. Fel'dman EB, Lacelle S (1996) Configurational averaging of dipolar interactions in magnetically diluted spin networks. J Chem Phys 5:2000–2010
38. Atsarkin VA, Vasneva GA, Demidov VV, Dzheparov FS, Odintsov BM, Clarkson RB (2000) Dipolar broadening and exchange narrowing of EPR lines from the paramagnetic centers distributed on a solid surface. JETP Lett 7:369–372
39. Dzheparov FS, Kaganov IV (2002) Resonance line shape in a magnetically diluted system of an arbitrary dimensionality. JETP Lett 6:259–263
40. Paul P, KCh KK, Sun D, PDW B, ChA R (2002) Artifacts in the electron paramagnetic resonance spectra of C60 fullerene ions: inevitable C120O impurity. J Am Chem Soc 124:4394–4401
41. Shames AI, Katz EA, Panich AM, Mogilyansky D, Mogilko E, Grinblat J, Belousov VP, Belousova IM, Ponomarev AN (2009) Structural and magnetic resonance study of astralen nanoparticles. Diam Relat Mater 18:505–510
42. Zaritskii IM, Ishchenko SS, Konchits AA, Kolesnik SP, Vorona IP, Okulov SM, Pokhodnya KI (1996) EPR, ENDOR, and spin relaxation in powdered fullerite. Phys Solid State 38:231–235
43. Grinberg OY, Williams BB, Runge AE, Grinberg SA, Wilcox DF, Swarts HM, Freed JH (2007) Oxygen effect on the EPR signals from wood charcoals: experimental results and the development of a model. J Phys Chem B 111: 13316–13324
44. Marciano O, Gonen S, Levy N, Teblum E, Yemini R, Nessim GD, Ruthstein S, Elbaz L (2016) Modulation of oxygen content in Graphene surfaces using temperature-programmed reductive annealing: electron paramagnetic resonance and electrochemical study. Langmuir 44:11672–11680